Boundary-Driven Colloidal Crystallization in Simple Shear Flow

Laura T. Shereda, Ronald G. Larson, and Michael J. Solomon*

University of Michigan, Ann Arbor, Michigan 48109-2136, USA

(Received 18 July 2010; revised manuscript received 27 September 2010; published 24 November 2010)

Using confocal microscopy, we directly observe that simple shear flow induces transient crystallization of colloids by wall-normal propagation of crystallization fronts from each shearing surface. The initial rate of the front propagation was 1.75 ± 0.07 colloidal layers per unit of applied strain. The rate slowed to 0.29 ± 0.04 colloidal layers per unit of applied strain as the two fronts approached each other at the midplane. The retardation of the front propagation is caused by self-concentration of shear strain in the growing bands of the lower-viscosity crystal, an effect that leads to a progressive reduction of the shear rate in the remaining amorphous material. These findings differ significantly from previous hypotheses for flow-induced colloidal crystallization by homogeneous mechanisms.

DOI: 10.1103/PhysRevLett.105.228302 PACS numbers: 47.57.J−, 47.85.mb, 83.10.Tv

Relative to quiescent conditions, shear flow significantly accelerates the crystallization of metastable, amorphous colloid suspensions [1]. The requirements for shear-induced crystallization are that the dimensionless applied shear stress, the Peclet number Pe be order one or greater: i.e., $\mathrm{Pe} = \tau_{yx} a^3/k_b T > 1$ [2]. Here τ_{yx} is the shear stress, a is the particle radius, and $k_b T$ is the thermal energy. This criterion was established by steady-state measurements in oscillatory and steady flows [3]. The kinetics of colloidal crystallization has received less attention. Recent work has addressed the effect of flow on crystallization kinetics through its modification of homogeneous mechanisms such as nucleation and growth [4–6]. However, because previous experiments have only probed overall crystallization rates, direct evidence of the mechanisms of flow-accelerated crystallization is lacking.

In this Letter, we use confocal microscopy to directly visualize the effect of shear flow on the kinetics of colloidal crystallization. Contrary to previous work, we observe that shear-induced crystallization is wall-nucleated and propagates as the strain is increased layer by layer in a direction normal to the shearing surface. The strain required for full crystallization scales with the gap between the shear surfaces. Initially, each layer of crystallized colloids added requires about 0.57 units of strain. This rate decreases as the two crystalline boundaries propagate in from each shearing surface and ultimately converge at the midplane of the shear flow. We use these new results to produce a model that predicts the kinetics of crystallization for this heterogeneous mechanism. Improved understanding of these kinetics can be applied to design flows, such as coating and roll-to-roll printing, to produce colloidal crystals on the large scales necessary for advanced material applications [7].

Early experimental studies of shear-induced colloidal crystallization used scattering [1], which can determine the critical shear stress for onset of crystallization. However, because scattering probes collective properties over a $\sim$ mm^3 volume, it cannot resolve spatial variation of microstructure below that scale. This limitation may now be addressed with confocal microscopy, which has been applied to understand shear-induced melting, nucleation and growth, shear banding, epitaxy, and the dynamics of grain boundaries [8–13].

We use confocal laser scanning microscopy (Leica SP2, $100 \times \mathrm{NA} = 1.4$ objective) to image monodisperse poly(methyl methacrylate) particles (diameter $2a = 0.68\ \mu\mathrm{m} \pm 2.3\%$) sterically stabilized with poly(12-hydroxystearic acid) [14], labeled with the fluorescent dye Nile red [15] and dispersed in the viscous, nonvolatile solvent dioctyl phthalate ($\mu = 0.718$ Pa · s at $T = 25\,^{\circ}\mathrm{C}$) with 10 μM of the weak electrolyte tetrabutylammonium-chloride [16]. The colloids are both sterically and charge stabilized, consistent with the liquid-crystal coexistence observed at $0.185 < \phi < 0.235$, where ϕ is the colloid volume fraction [16]. Experiments were performed in the fully crystalline region of the phase diagram.

Approximately 100 μl of a $\phi = 0.35$ suspension was loaded into the gap of a shear cell with a stationary bottom plate and a moveable top plate [17] and mounted on the confocal laser scanning microscopy. Plates were coated with melted poly(methyl methacrylate) ($\sim 1\ \mu$m thick) to eliminate any slip flow and were aligned to a parallelism of at least 0.2 μm gap dimension per millimeter of travel. Direct visualization and image analysis showed that sample loading induced neither crystallization nor density gradients in the shear cell gap. The time between loading and step strain was less than 200 s, much faster than the quiescent crystallization time of $\sim 10^4$ s for this system [18]. The gap was adjusted from 50 to 250 μm. At a typical gap of 150 μm, the strain for full travel was $\gamma = L/H \sim 66$, where L is the full travel and H is the gap. At this gap, the applied shear rate could be varied from 0.05 to 0.5 s^{-1}. Given the measured shear-rate dependent viscosity [17], these conditions correspond to Pe from 5 to 50. At a rate of 2.1 s^{-1} (Pe = 91), a transition to no

crystallization (shear melting) was observed. Particle-tracking image analysis of the velocity profile in the gap showed that flow was homogeneous for dilute suspensions. However, shear banded flow occurred for the $\phi = 0.35$ conditions studied here. In this case, the shear rate of the crystalline region was significantly greater than in the amorphous region [17].

Because more than 100 colloidal layers are imaged after strains greater than 100 units, real time confocal microscopy imaging methods [19] are not feasible. Instead, after shear, UV photopolymerization [7% photopolymer (CD501, Sartomer) and 1% photoinitiator (Irgacure 2100, Ciba Specialty)] of the solvent was performed [18] to rapidly immobilize ($t < 0.5$ s) the colloidal structure. Because dioctyl phthalate is viscous, immobilization was much faster than colloidal diffusion [18]. Five $30 \times 30 \times 75$ μm^3 image volumes were collected with voxel size $59 \times 59 \times 77$ nm^3. Particles were located [15] to ± 35 nm in the objective plane and ± 45 nm along the axis normal to the objective plane [15]. Local crystallinity was quantified with frame-invariant bond-order parameters [15,20] applied to the nearest neighbors within $r = 1.41$ μm. Although different crystalline structures [21] and stacking faults [22] can be resolved, here we focus on the spatial distribution of amorphous and crystalline structures.

Figure 1 reports the results at Pe $= 23.3$ and 150 μm gap. The suspension was initially amorphous [Fig. 1(a)]. In Fig. 1(b), after an applied strain $\gamma = 40$, the sample is partially crystalline and a sharp boundary between a crystalline region close to the wall and a noncrystalline region away from the wall is apparent. Upon $\gamma = 160$, the sample is fully crystalline [Fig. 1(c)]. A 3D rendering of crystalline and amorphous particles is shown in Fig. 1(d) ($\gamma = 40$). The results confirm that the near-wall layers of the suspension crystallized first and that a rather sharp boundary separates these from the amorphous material further into the sample. Although data here are from the bottom half of the sample, direct visualization above and below the midplane showed that the crystallization behavior was symmetric about that midplane (data not shown). The sample near the shearing surface is nearly fully crystalline ($X > 0.8$) at $\gamma = 40$; see Fig. 1(e). At a distance from the shear surface of $\sim$45 μm, the specimen transitions from crystalline to noncrystalline ($X < 0.05$) within a distance $\sim$5 μm. The observation of a crystalline front differs from the homogeneous mechanisms that have previously been used to explain the accelerated kinetics of shear-induced crystallization [5,6].

These methods were repeated at nine different values of the strain (at Pe $= 23.3$) to produce Fig. 2. For small strains ($\gamma < 10$), crystallization occurs only in the near-wall region ($h < 10$ μm) and only to a small degree ($X < 0.4$). At $\gamma \sim 25$ there is an abrupt transition from crystalline to noncrystalline layers that migrates further from the shearing boundary with increased strain up to $\gamma \sim 125$. At $\gamma = 160$, the crystalline boundaries propagating from

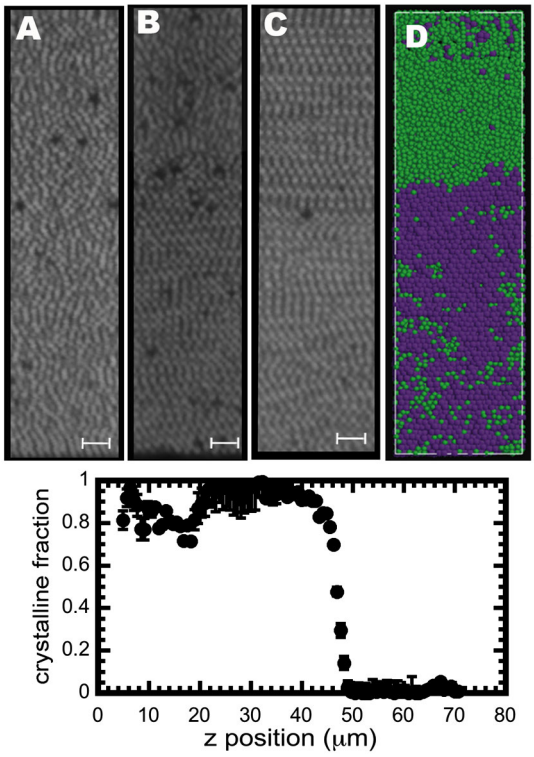

FIG. 1 (color online). 2D cross section of a 3D confocal laser scanning microscopy image volume showing the colloidal microstructure before flow (a), at $\gamma = 40$ (b), and after $\gamma = 160$ (c). The cross sections are orthogonal to the flow direction and extend from the lower shearing surface to the midplane of the flow. The scale bars are 5 μm, the gap is 150 μm, and Pe $= 23.3$. (d) Rendering for $\gamma = 40$ showing noncrystalline (green or light gray) and crystalline (purple or dark gray) particles. (e) Plot of the wall-normal variation in crystal quality for $\gamma = 40$.

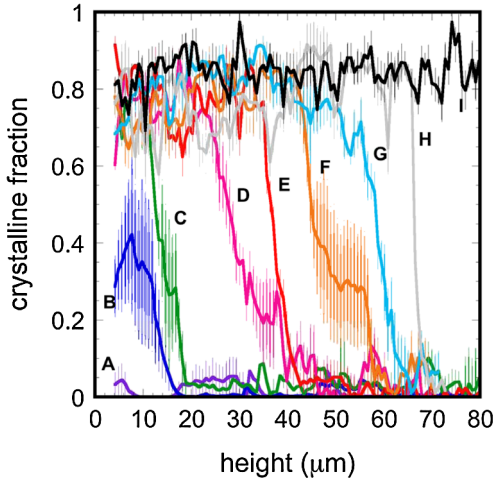

FIG. 2 (color online). The wall-normal variation in crystallinity for different applied step strains. All experiments were performed at a gap of 150 μm and Pe $= 23.3$. Each curve is the average of five samples, and error bars are the standard error of the mean. From left to right, the applied step strains are 1, 2, 10, 25, 40, 75, 100, 125, and 160.

the top and bottom surfaces have converged at the flow midplane, and the specimen is fully crystalline ($X > 0.85$) everywhere. The results indicate that new crystalline layers are deposited onto a plane of existing layers via epitaxial deposition [11,12] with shear strain apparently providing the energy needed to overcome a free energy barrier to deposition and thereby greatly accelerating the crystallization relative to equilibrium conditions.

A characteristic height of the crystalline boundary was taken as the point at which $X = 0.5$ in Fig. 2 and plotted in Fig. 3(a). Additional measurements at Pe = 8 and Pe = 45 show that the front propagation is independent of shear rate within this range of Pe. Figure 3(a) shows a nonlinear dependence of the crystalline boundary on the applied strain. Figure 3(b) shows that this nonlinear dependence is found for a wide range of gaps. Thus, the crystal boundary propagation depends on the shear-flow gap (or, in dimensionless terms, the ratio of the gap to the colloid diameter, $H/2a$) as well as the applied strain.

Figure 4 is a master curve for all the data found when h^*, the crystalline boundary height, is scaled with the gap H and when the applied strain is scaled on the dimensionless gap height ($H/2a$). The crystallization growth rate is highest initially. Quadratic extrapolation of the Fig. 4 data for $\gamma^* 2a/H < 0.3$ finds this initial growth rate $V_{\text{initial}} = (1.75 \pm 0.07)^* 2a$. Here $2a$ is the particle diameter, and V_{initial} is the initial change in crystal height per unit of applied strain. This rate progressively slows until at the midplane its value is $V_{\text{midplane}} = (0.29 \pm 0.04)^* 2a$.

Figure 4 establishes a dependence of shear-induced crystallization kinetics on both the applied strain and the gap. Two physical effects produce the dependence on gap. First, because the initial growth rate is independent of gap, larger gaps require more strain for crystallization. Second, as shown by Fig. 4, the progressive decrease in the crystallization rate scales with the gap H. This scaling suggests

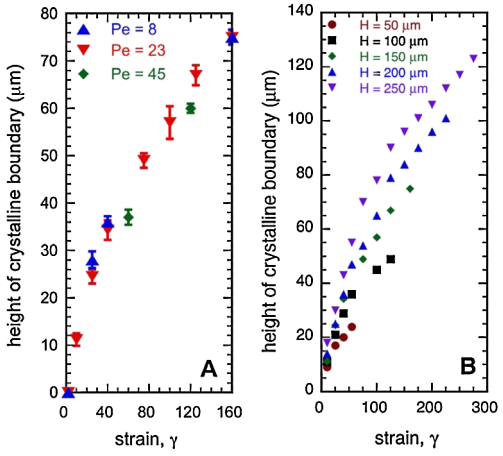

FIG. 3 (color online). (a) Strain dependence of crystal quality for varying Peclet numbers. Each point is the average height of the crystalline boundary from five samples. (b) Gap dependence of crystalline front propagation. The data are all at an applied shear rate of 0.266 s^{-1} (Pe = 23.3).

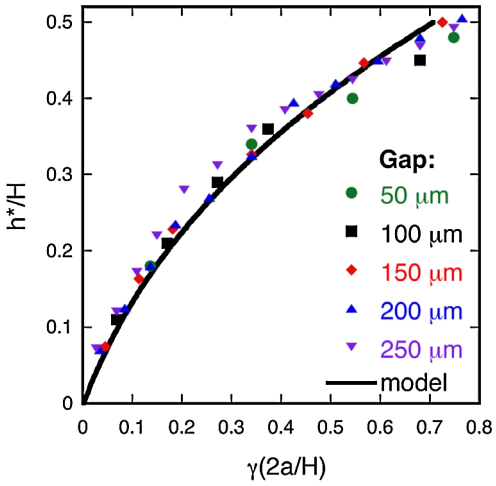

FIG. 4 (color online). Scaled master curve for the strain dependence of colloidal crystallization kinetics in simple shear flow. The curve is the model based on measurements of the front growth rate V and the viscosity ratio M.

a hydrodynamic mechanism for the progressive decrease in the crystallization front velocity. Indeed, as discussed earlier, particle tracking velocimetry found that the flow was shear-banded, that the degree of banding was strain-dependent, and that the band location correlated with the crystallization boundary [17].

We hypothesize that the crystallization front growth rate is proportional to the strain in the amorphous region:

$$d(h^*) = V d\gamma_{\text{amorphous}}. \tag{1}$$

From the data, the growth rate $V = (1.75 \pm 0.07)^* 2a$, because initially the flow is fully amorphous. Because the shear rates in the crystalline and amorphous regions differ, the shear strain in the amorphous region of the flow differs from the applied strain. The shear rates in the crystalline and amorphous shear bands are connected by the homogeneity of stress:

$$\frac{\dot{\gamma}_{\text{crystalline}}}{\dot{\gamma}_{\text{amorphous}}} = \frac{\eta(\dot{\gamma})_{\text{amorphous}}}{\eta(\dot{\gamma})_{\text{crystalline}}} = M(\gamma_{\text{applied}}), \tag{2}$$

where M is the ratio of the viscosity in the amorphous and crystalline bands. The shear rates in the crystalline and amorphous bands differ as well. Continuity of velocity at the boundary of the bands, along with Eq. (2), requires that the crystalline and amorphous band shear rates satisfy

$$\dot{\gamma}_{\text{applied}}\left(\frac{H}{2}\right) = \dot{\gamma}_{\text{crystalline}} h^* + \dot{\gamma}_{\text{amorphous}}\left(\frac{H}{2} - h^*\right). \tag{3}$$

(This equation captures the symmetry of the flow about the midplane.) Finally, the strain in the amorphous band, which determines the growth of the crystalline front from Eq. (1), is given by

$$\gamma_{\text{amorphous}} = \int_0^{\gamma_{\text{applied}}} d\gamma_{\text{amorphous}} = \int_0^{\gamma_{\text{applied}}} \left((M-1)\frac{2h^*}{H}+1\right)^{-1} d\gamma_{\text{applied}}. \quad (4)$$

The viscosity ratio M was measured with cone and plate rheometry over the shear-rate range of the transient flow ($0.06\ \text{s}^{-1} < \dot{\gamma} < 0.8\ \text{s}^{-1}$). M varied from 3.0, initially, to 4.4, finally. The measured velocity field is consistent with this viscosity ratio range [17]. From the model, the amorphous shear rate decreases by more than a factor of 4 from initial to full crystallization.

Given the measured V and M, the model is completely specified, and its prediction is plotted in Fig. 4. The excellent agreement indicates that both the effect of the front-propagation rate V and the effect of shear banding, as quantified by the differing viscosities of the amorphous and crystalline phases M, are required to quantitatively predict the strain requirements of the crystallization kinetics. Physically, the growth rate per unit of applied strain progressively decreases because the strain rate in the amorphous layer decreases as the crystalline layer grows. The amorphous strain is reduced because of the low strain rate in this layer due to its greater viscosity relative to the crystalline phase. Note in Fig. 4 the slight negative deviation of the data, largest for the two smallest gaps, at high strain. We suggest that this deviation is due to a slowing-down of crystallization when the two fronts from opposing walls collide and fuse. This slowing-down would affect only a few central layers and thus have the largest relative effect for the smallest dimensionless gaps, as observed.

Thus, a wall-nucleated crystallization front explains the kinetics of crystallization of submicron colloids in simple shear flow, at least up to the gaps of 0.25 mm studied here (about 370 times the colloid diameter) for the case of $\text{Pe} > 1$. Thus, previously hypothesized homogeneous mechanisms must be slower than the front-propagation mechanism for gaps of this dimension and smaller, since no evidence of the former mechanism was observed. It remains unresolved if homogeneous mechanisms might be directly observed in flows of larger gap to particle diameter ratio [5].

In the case of large gaps, the crystalline front would require more units of strain (and thus a longer time) to propagate to the midplane of the shear flow. For example, for the shear flow of ~400 nm diameter colloids within a 2 mm gap as in Ref. [5], our model would predict ~3500 strain units for full crystallization by the wall-normal front-propagation mechanism. Because this predicted strain is greater than was observed [5], as the gap is increased there ought to be a crossover from the mechanisms reported in this work, to those reported in Refs. [5,6]. Our work thus shows that theory and modeling of shear-induced colloidal crystallization must account for heterogeneous, wall-nucleated mechanisms, in addition to the previously studied homogeneous mechanisms [5,6] and nonequilibrium effects [23]. Finally, we highlight that an explanation for the particular magnitude of the observed front-propagation rate ($V = 1.75 \pm 0.07$ colloidal diameters per unit of applied strain) is currently lacking, although a strain of order unity is not surprising, since a displacement of one particle diameter, in principle, should allow each particle to find its place within a planar lattice.

This study was supported by the National Science Foundation (NSF CBET 0707383).

*mjsolo@umich.edu

[1] J. Vermant and M. J. Solomon, J. Phys. Condens. Matter **17**, R187 (2005).
[2] B. J. Ackerson, J. Rheol. **34**, 553 (1990).
[3] L. B. Chen, B. J. Ackerson, and C. F. Zukoski, J. Rheol. **38**, 193 (1994).
[4] S. Butler and P. Harrowell, J. Chem. Phys. **103**, 4653 (1995).
[5] P. Holmqvist, M. P. Lettinga, J. Buitenhuis, and J. K. G. Dhont, Langmuir **21**, 10 976 (2005).
[6] R. Blaak, S. Auer, D. Frenkel, and H. Lowen, Phys. Rev. Lett. **93**, 068303 (2004).
[7] V. L. Colvin, MRS Bull. **26**, 637 (2001).
[8] V. Prasad, D. Semwogerere, and E. R. Weeks, J. Phys. Condens. Matter **19**, 113102 (2007).
[9] Y. L. Wu, D. Derks, A. van Blaaderen, and A. Imhof, Proc. Natl. Acad. Sci. U.S.A. **106**, 10 564 (2009).
[10] V. W. A. de Villeneuve, R. P. A. Dullens, D. G. A. L. Aarts, E. Groeneveld, J. H. Scherff, W. K. Kegel, and H. N. W. Lekkerkerker, Science **309**, 1231 (2005).
[11] A. van Blaaderen, R. Ruel, and P. Wiltzius, Nature (London) **385**, 321 (1997).
[12] R. Ganapathy, M. R. Buckley, S. J. Gerbode, and I. Cohen, Science **327**, 445 (2010).
[13] A. M. Alsayed, M. F. Islam, J. Zhang, P. J. Collings, and A. G. Yodh, Science **309**, 1207 (2005).
[14] L. Antl, J. W. Goodwin, R. D. Hill, R. H. Ottewill, S. M. Owens, and S. Papworth, Colloids Surf. **17**, 67 (1986).
[15] C. J. Dibble, M. Kogan, and M. J. Solomon, Phys. Rev. E **74**, 041403 (2006).
[16] C. P. Royall, M. E. Leunissen, and A. van Blaaderen, J. Phys. Condens. Matter **15**, S3581 (2003).
[17] L. T. Shereda, R. G. Larson, and M. J. Solomon, Korea-Australia Rheol. J. (to be published).
[18] L. T. Shereda, R. G. Larson, and M. J. Solomon, Phys. Rev. Lett. **101**, 038301 (2008).
[19] D. Derks, Y. L. Wu, A. van Blaaderen, and A. Imhof, Soft Matter **5**, 1060 (2009).
[20] P. R. ten Wolde, M. J. Ruiz-Montero, and D. Frenkel, J. Chem. Phys. **104**, 9932 (1996).
[21] U. Gasser, E. R. Weeks, A. Schofield, P. N. Pusey, and D. A. Weitz, Science **292**, 258 (2001).
[22] T. Solomon and M. J. Solomon, J. Chem. Phys. **124**, 134905 (2006).
[23] J. Delhommelle, Phys. Rev. E **71**, 016705 (2005).